ACS MATERIALS LETTERS

www.acsmaterialsletters.org

LETTER

Erythrocyte-Membrane-Camouflaged Nanocarriers with Tunable Paclitaxel Release Kinetics via Macromolecular Stereocomplexation

Yen-Nan Lin, Mahmoud Elsabahy, Sarosh Khan, Fuwu Zhang, Yue Song, Mei Dong, Richen Li, Justin Smolen, Rachel A. Letteri, Lu Su,* and Karen L. Wooley*

Cite This: *ACS Materials Lett.* 2020, 2, 595–601

Read Online

ACCESS | Metrics & More | Article Recommendations | Supporting Information

ABSTRACT: Biomimetic-cell-membrane-camouflaged polymeric nanocarriers, possessing advantages related to the functional diversity of natural cell membranes and the physicochemical tailorability of synthetic polymers, serve as promising candidates for a therapeutic platform. Herein, we report a facile approach for the fabrication of erythrocyte (red blood cell, RBC)-membrane-camouflaged nanocarriers (RBC-MCNs) that exhibit tunable paclitaxel (PTX) release kinetics via altering macromolecular stereostructure. In this approach, biocompatible isotactic and atactic polylactides (PLAs) with similar molar masses (M_n = 8.2−8.9 kDa, as measured by NMR spectroscopy) and dispersities ($Đ$ < 1.1, as measured by size exclusion chromatography) were synthesized via organocatalyzed ring-opening polymerizations (ROPs), providing tunable crystalline structures via polymer tacticity, while RBC membranes provided biomimetic surfaces and improved colloidal stability of PLA nanoconstructs in phosphate-buffered saline (PBS, pH 7.4). Wide-angle X-ray diffraction (WAXD) and differential scanning calorimetry (DSC) analyses of the lyophilized nanoconstructs suggested significant retention of PLA stereocomplexation upon loading the hydrophobic anticancer drug PTX, enabling control over drug release kinetics. The structure−property relationships were maintained after the RBC coating, with 100% stereocomplexed PLA RBC-MCNs exhibiting the least PTX release during the first 12 h in PBS at 37 °C, compared to 2-, 3-, and 4-fold higher amounts of release for the 50% stereocomplexed, isotactic, and amorphous PLA counterparts, respectively. The extended release of PTX from the 100% stereocomplexed PLA RBC-MCNs resulted in an increased IC_{50} (0.50 μM) against SJSA osteosarcoma cells, relative to amorphous PLA RBC-MCNs (IC_{50} = 0.25 μM) or free PTX (IC_{50} = 0.05 μM). In contrast, non-PTX-loaded RBC-MCNs were not cytotoxic, and they also displayed lower immunotoxic responses against RAW 264.7 macrophage cells compared to RBC membrane vesicles. This work represents fundamental advances toward a potential personalized nanocarrier technology that would be capable of employing an individual's RBCs for membrane isolation, together with tuning of cargo loading and release simply via alteration of the biocompatible PLA stereoisomer feed ratio.

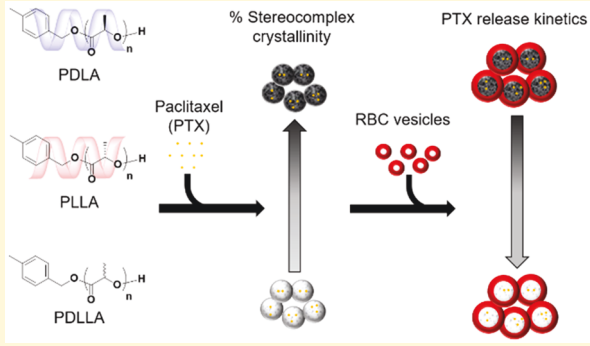

Cell-membrane-camouflaged polymeric nanocarriers (MCNs) combine advantages related to the functional diversity of natural cell membranes and the physicochemical tailorability of synthetic polymers.[1−4] Many studies have focused on utilizing diverse cell-derived membranes to functionalize nanocarrier surfaces, leading to biomimetic nanocarriers with different surface properties toward various applications, including drug delivery,[5] vaccination,[6] toxin neutralization,[7−9] anti-inflammatory agents,[10] photothermal therapy,[11] and cancer immunotherapy.[12−14] Erythrocyte (red blood cell, RBC)-membrane-camouflaged nanoparticles (RBC-MCNs) have been shown to decrease protein adsorption, reduce immune response, and prolong blood circulation times, compared to uncloaked nanoparticle counterparts.[1,15]

Received: February 7, 2020
Accepted: April 27, 2020
Published: April 30, 2020

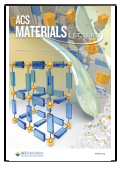

https://dx.doi.org/10.1021/acsmaterialslett.0c00044
ACS Materials Lett. 2020, 2, 595−601

Scheme 1. Design of the RBC-Membrane-Camouflaged Nanocarriers with Tunable Drug Release Kinetics

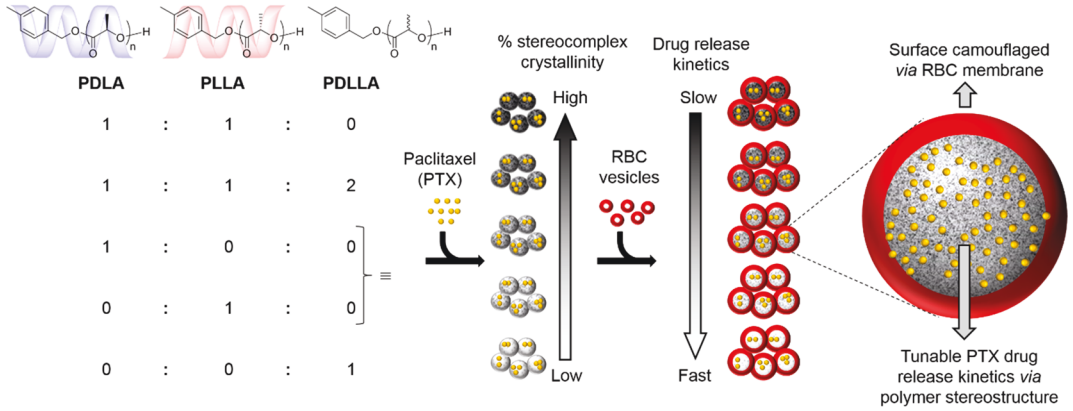

Controlling cargo release kinetics is essential for the optimization of MCNs toward various applications. Tuning cargo release kinetics is particularly crucial for drug delivery to maintain optimal drug concentration duration, reduce side-effects, and improve therapeutic efficacy.[16] Altering core compositions of the nanocarrier can influence drug release kinetics,[17−19] yet many tailor-made materials have unknown toxicity profiles in humans, increasing the uncertainty for clinical translation of the resulting MCNs. Expanding control over the drug release kinetics for MCNs using biocompatible materials is, therefore, desirable.

Non-covalent polylactide (PLA) stereocomplex interactions can provide a versatile strategy to tune the drug release kinetics, while the surface chemistry is also important in the overall characteristics and performance of MCNs as drug delivery devices. PLA homopolymer, a biocompatible and biodegradable aliphatic polyester, has been FDA-approved as a medical implant material for anchors, screws, plates, pins, rods, and meshes.[20,21] Physical blending of isotactic and enantiomeric poly(D-lactide) (PDLA) and poly(L-lactide) (PLLA) forms regular stereocomplexes with increased crystallinity, leading to higher melting transition temperatures and greater mechanical strength, compared to the isotactic counterparts.[22−24] PLA crystalline domains are analogous to non-covalent cross-linking within a polymer matrix. Core cross-linked polymer nanoconstructs reduce drug release rates by hindering drug diffusion.[25,26] Tuning drug release kinetics with PLA stereocomplexation has been reported in PEG−PLA platforms for drugs, such as doxorubicin,[27] camptothecin,[28] and rifampin.[29,30] However, with replacement of PEG by a RBC-membrane-based coating material, MCNs outperformed PEGylated counterparts in recent literature, with double blood circulation half-life.[1,15] MCNs also offer diverse biointerfaces by employing different biological membrane components, beyond those found on RBCs, to exhibit affinities to various biological targets that range from toxins,[7] to damaged vasculature,[31] to cancer cells,[11] and to microbes.[31] In contrast, installing such a variety of biomimetic moieties onto a PEGylated surface could be a costly and labor-intensive process. Furthermore, PEGylated nanoparticles (NPs) can elicit an immune response, leading to accelerated blood clearance with repeated administrations.[32,33] The present study combines these two concepts and provides a facile fabrication method for MCNs with tunable drug release kinetics via internal macromolecular stereostructure using biocompatible amorphous, crystalline, and stereocomplexed PLA materials and external surface chemistry derived from RBC membranes (Scheme 1).

Isotactic PDLA, PLLA, and atactic PDLLA were synthesized via organocatalyzed ring-opening polymerizations (ROP) of cyclic lactide (D-lactide, L-lactide, and DL-lactide, respectively) at −78 °C in dichloromethane (DCM) with 4-methylbenzyl alcohol as the initiator and 1,5,7-triazabicyclo[4.4.0]dec-5-ene (TBD) as the organocatalyst. The structures of PLAs were confirmed by ^{1}H NMR (Figure S1), ^{13}C NMR (Figures S2−S4), and FT-IR (Figure S5) spectroscopies, and the thermal properties were evaluated by thermogravimetric analysis (TGA, Figure S6). Size exclusion chromatography (SEC) indicated a monomodal molar mass distribution with low dispersity ($Đ$ < 1.1) of each polymer, demonstrating the well-defined structures (Figure S7). The number-averaged molar mass (M_n) of the polymers and degrees of polymerization (DP_n) were calculated from the ^{1}H NMR spectra (Figure S1), acquired after isolation of the polymer samples by precipitation. For each, comparison of the integral of the methyl protons originating from the initiator at 2.35 ppm with that of methyl groups from the repeating units at 1.58 ppm allowed for calculation of the DP_n, which was then converted to a value of M_n by multiplying the molar mass of the repeat unit (144 Da) by the DP_n and adding the molar mass of the chain ends. The resulting polymers showed comparable M_n (8.4 kDa for PDLA, 8.2 kDa for PLLA, and 8.9 kDa for PDLLA), thus minimizing the effects of molar mass variations in the study.

A series of PLA NPs with varying degrees of stereocomplexation was fabricated through a nanoprecipitation strategy. Briefly, a PLA solution with a predetermined enantiomeric ratio of PDLA vs PLLA vs PDLLA in THF (1 mg/mL) was added drop-wise (6 mL/h) into nanopure water under stirring (300 rpm) via a syringe pump. The 100% stereocomplexed PLA (scPLA) NPs contained a 1:1 mass ratio of PDLA and PLLA, whereas 50% stereocomplexed PLA (50% scPLA) NPs contained a 1:1:2 mass ratio of PDLA:PLLA:PDLLA (Table S1). NPs containing neat crystalline PDLA or PLLA and amorphous PDLLA were also prepared. Similarly, the same procedure was conducted for each of the five polymer stereostructure formulations, with PTX (at 5 and 10 wt %) added to the THF solution prior to nanoprecipitation into water. It is noteworthy that the rather low initial THF-to-water volume ratio (1:10) and the fast stirring rate ensured the formation of well-defined nanoscale stereocomplexes.[34] The final polymer concentration was subsequently adjusted to 0.5 mg/mL with nitrogen-flow-promoted evaporation. The resulting PLA NPs

https://dx.doi.org/10.1021/acsmaterialslett.0c00044
ACS Materials Lett. 2020, 2, 595−601

were similar in size regardless of the core stereostructures, with the number-average hydrodynamic diameter ($D_{h(number)}$) ranging from 70 to 90 nm for the neat polymer samples (Figure S8), and slightly larger sizes with PTX loading (*vide infra*).

The nature of the PLA as stereocomplexed, crystalline, and/or amorphous structures was confirmed by wide-angle powder X-ray diffraction (WAXD) and Fourier transform infrared (FT-IR) analyses of the lyophilized PLA NPs as a function of the PLA stereochemistries employed during the nanoprecipitation process (Figure 1 and Figure S5). As depicted in Figure 1,

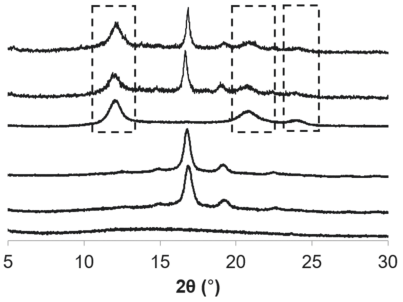

Figure 1. Wide-angle X-ray diffraction of the lyophilized PTX-loaded and empty PLA NPs, indicating partial retention of stereocomplexation upon PTX loading. From top to bottom: 10 wt % PTX-loaded scPLA, 5 wt % PTX-loaded scPLA, scPLA, PDLA, PLLA, and PDLLA NPs. The dashed rectangle encloses XRD peaks that are associated with the PLA stereocomplex crystalline domains.

atactic PDLLA assemblies did not exhibit distinct diffraction patterns, indicating no significant crystalline domains, as expected for an amorphous structure. Isotactic PDLA and PLLA NPs showed identical diffraction patterns (2θ = 15, 17, 19, and 22.5°), revealing similar crystal packing within the polymer matrix. Stereocomplexed PLA co-assemblies showed differences in X-ray diffraction patterns (2θ = 12, 21, and 24°) compared to those of the isotactic NPs, suggesting changes in crystal structures and formation of PLA stereocomplex equilateral-triangle-shaped crystals.[35−37] PLA stereocomplex formation was further evidenced by FT-IR, with the appearance of the characteristic peak at 908 cm^{-1} (Figure S5).[38]

Colloidal stability upon drug (paclitaxel, PTX) loading was further investigated in both nanopure water and phosphate-buffered saline (PBS, pH 7.4), since the additional hydrophobicity introduced by PTX could have resulted in secondary aggregation or precipitation. Upon loading hydrophobic PTX (5 wt %, 67−86% loading efficiency as measured by HPLC, Table S2), colloidally stable (>1 week) PTX-loaded PLA NPs were obtained with dry-state average diameters (D_{av}) ranging from 63 to 69 nm, as measured by transmission electron microscopy (TEM), and $D_{h(number)}$ of 110−130 nm, according to DLS, independent of the PLA stereochemistry (Figure S9). However, PTX-loaded bare PLA NPs immediately precipitated in PBS (Figure 3c), and bare PLA NPs were known to be extensively endocytosed by monocytes in plasma,[39] suggesting bare PLA NPs alone cannot serve as drug nanocarriers.

The crystalline properties of the PTX-loaded PLA NPs were subsequent evaluated by WAXD and DSC, since loading hydrophobic drug could potentially disrupt non-covalent intermolecular interactions within the polymer matrix, specifically crystallinity and stereocomplexation crystallinity. As depicted in Figure 1, upon loading PTX in scPLA NPs, the X-ray diffraction analyses revealed the co-existence of the stereocomplex-associated diffraction patterns and the non-stereocomplex-associated diffraction pattern, regardless of PTX loading amount (5 or 10 wt %). This observation indicated partial stereocomplex disruption, resulting in heterogeneous stereocomplex and isotactic PLA crystalline domains in the polymer matrix. DSC analyses of the lyophilized PLA nanoconstructs further supported partial stereocomplex retention upon PTX loading (Figure 2). Since thermal history can be

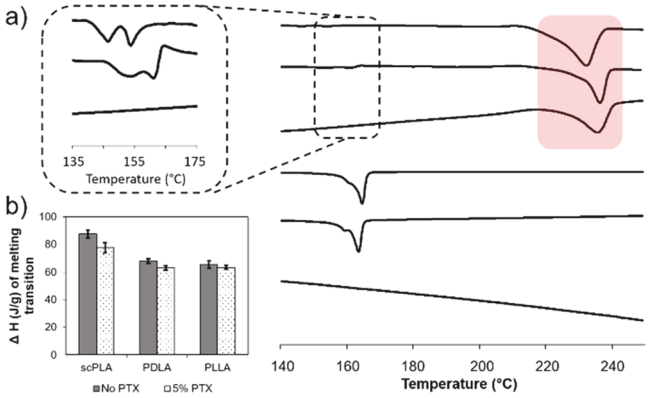

Figure 2. Thermal analysis of the lyophilized PTX-loaded and empty PLA NPs indicated the retention of stereocomplexation upon PTX loading. From top to bottom: 10 wt % PTX-loaded scPLA, 5 wt % PTX-loaded scPLA, scPLA, PDLA, PLLA, and PDLLA NPs. Traces were taken from the first heating cycle. (a) The PLA stereocomplex melting transition is highlighted. The dashed rectangle encloses an enlarged view of the non-stereocomplex isotactic PLA melting transition. (b) Comparison of the enthalpies (ΔH) of PLA melting transitions with or without 5 wt % PTX loading.

introduced during heating−cooling processes (Figure S10), only the first heating cycle of the DSC traces, which contained relevant information associated with polymer packings of the as-prepared nanoconstructs, was analyzed to decipher the effect of PTX loading on the PLA polymer packing. The atactic PDLLA NPs exhibited a glass transition temperature (T_g) at 56 °C with no melting transition (T_m), as expected for an amorphous material. Isotactic PDLA and PLLA NPs displayed T_m transitions at 167 and 164 °C, respectively, whereas 100% stereocomplex PLA NPs exhibited a single T_m at 232 °C, which was 65−68 °C higher than the T_m of PDLA or PLLA NPs, suggesting the formation of a stereocomplex interaction.[36,40] The PLA stereocomplex melting transition was retained upon PTX loading (5 and 10 wt %). Upon further analyses of the 135−175 °C regions of the PTX-loaded scPLA thermograms, two small melting transitions were observed corresponding to the isotactic PLLA and PDLA crystalline regions (Figure 2a), indicating the slight interference of the well-defined equilateral-triangle-shaped crystal. However, qualitatively, the melting transition enthalpies of PLA NPs underwent minimal reduction upon hydrophobic PTX loading, suggesting significant crystallinity retention (Figure 2b).

To improve solution stability and provide biomimetic surface moieties, RBC membrane vesicles were used to coat PTX-loaded PLA NPs and afford RBC-MCNs with different core tacticities, using reported protocols (Figure 3 and Figures S9, S11, and S12).[31,41] Briefly, PLA NPs (1 mg) and RBC membrane vesicles (derived from 150 μL of human blood) were mixed and sonicated for 10 min in a capped glass vial using a VWR 75T bath sonicator, followed by stirring at 4 °C for 1

https://dx.doi.org/10.1021/acsmaterialslett.0c00044
ACS Materials Lett. 2020, 2, 595−601

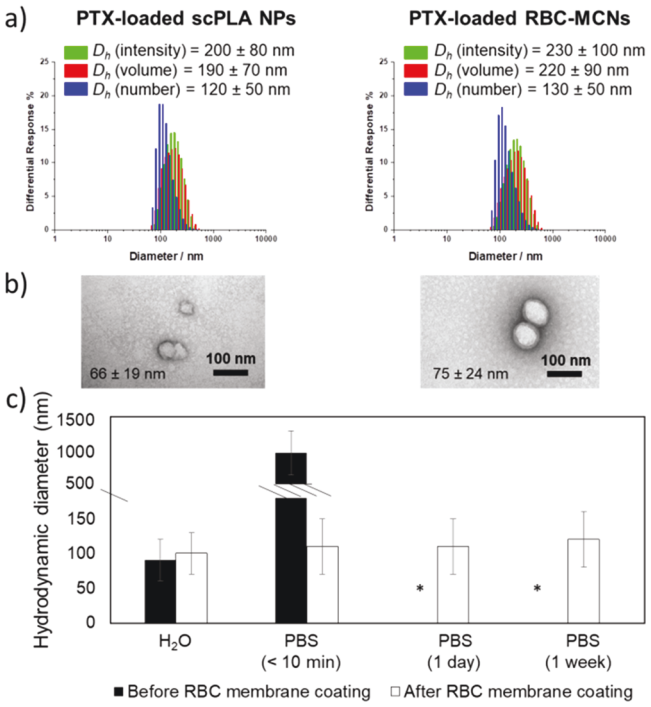

Figure 3. RBC membrane coating of the scPLA NPs was verified by (a) DLS, (b) TEM (samples negatively stained by 2% uranyl acetate with an average diameter (n = 50), and (c) colloidal stability in PBS (pH 7.4) at 4 °C with * indicating precipitation.

h.[15,42] The resulting PTX-loaded RBC-MCNs showed D_{av} values of 75−78 nm (as measured by TEM) and $D_{h(number)}$ values of 130−140 nm (as measured by DLS, Figure S9). The increase in diameter (ca. 10 nm) indicated the successful coating of two layers of RBC membrane with each layer thickness of 5 nm (Figure 3a and b).[43] The zeta potential was changed from ca. −40 mV to ca. −10 mV after RBC membrane coating, owing to the difference in surface charge density between PLA NPs and RBC membrane vesicles (Figure S11). Colloidal stability provided additional evidence for successful PTX-loaded RBC-MCN fabrication. In contrast to the behavior of PTX-loaded PLA NPs, which readily formed precipitates in PBS (pH 7.4) within a few minutes, PTX-loaded RBC-MCNs remained colloidally stable for a prolonged period (>1 week) at 4 °C (Figure 3c).

The structure−property relationships of PTX-loaded RBC-MCNs were evaluated by drug release profiles (Figure 4). An array of PTX-loaded RBC-MCNs was fabricated, and PTX release was monitored in PBS (pH 7.4) at 37 °C using HPLC. Since bare PTX-loaded PLA NPs precipitated immediately in PBS (Figure 3c), only RBC-MCNs were examined in the release study. The PTX-loaded RBC-MCNs showed sustained PTX release, with 100% stereocomplexed PLA RBC-MCNs exhibiting the least PTX release during the first 12 h, compared to 2-, 3-, and 4-fold higher amounts of release for the 50% stereocomplexed, isotactic, and amorphous PLA counterparts, respectively (Figure 4). After 8 days, RBC-MCNs with scPLA, 50%scPLA, PLLA, PDLA, and amorphous PLA cores released 27, 40, 54, 57, and 69% of the loaded PTX, respectively. These data demonstrate that the drug release kinetics of RBC-MCNs were successfully controlled by altering the core stereostructure of the MCNs. The densely packed PLA chains within the stereocomplexed core domains limited PTX diffusion and release; therefore, RBC-scPLA exhibited 10-fold (IC_{50} = 0.50

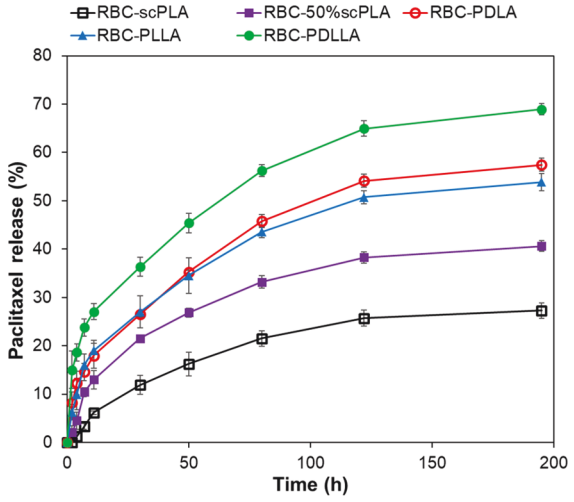

Figure 4. Release of PTX from PTX-loaded RBC-MCNs (5 wt %) studied by a dialysis method over 8 days at 37 °C in PBS buffers (pH 7.4), measured in triplicates.

μM) lower cytotoxicity in human osteosarcoma cells (SJSA-1) compared to free PTX (IC_{50} = 0.05 μM). The faster release of PTX from the amorphous cores of PTX-loaded RBC-PDLLA resulted in only a 5-fold reduction in cytotoxicity (IC_{50} = 0.25 μM) relative to the free small molecule drug (Figure S13). The sustained PTX release over prolonged periods could help maintain a persistent drug concentration in tumor tissues and improve therapeutic efficacy.[16] As a control, empty RBC-MCNs did not show significant cytotoxicity after incubation with SJSA-1 osteosarcoma cells for 72 h at a NP concentration range of 0.17−167 μg/mL (Figure S14).

The immunotoxicities of the RBC-MCNs were investigated by cytokine expression levels, which can demonstrate the ability of biomaterials to interact with the immune system, either *in vitro* or *in vivo*.[44,45] No significant overexpression of any of the tested 23 cytokines was observed for the PDLLA and scPLA NPs. On the contrary, the human-derived RBC membrane vesicles induced acute immunotoxic reactions in the RAW 264.7 mouse macrophage cell line, possibly due to foreign antigen recognition, as indicated by the significant overexpression (p = 0.03) of the G-CSF, IL-10, RANTES, and TNF-α (out of the 23 measured cytokines). Interestingly, acute immunotoxic responses against foreign membrane-associated antigens were reduced after coating the membrane onto the PLA NPs (Figure 5), potentially via altering the interaction of antigens with the surrounding biomolecules and receptors;[46] further study will be conducted to elucidate this phenomenon.

To conclude, we demonstrated a facile fabrication of RBC-MCNs with tunable PTX release kinetics via controlling the macromolecular stereostructure. Isotactic and atactic PLAs of similar molar masses (M_n = 8.2−8.9 kDa) and dispersities (<1.1) were synthesized via organocatalyzed ROPs. PLA assemblies, with varying polymer tacticity, had comparable hydrodynamic diameters. Significant PLA stereocomplex retention upon loading PTX was evidenced by WAXD and DSC experiments. The PTX release kinetics from the RBC-MCNs was successfully tuned by changing PLA stereochemistry, with a higher degree of stereocomplexation corresponding to slower PTX release. RBC-MCNs were not cytotoxic and displayed lower immunotoxic responses compared to the RBC membrane vesicles. This strategy can be

https://dx.doi.org/10.1021/acsmaterialslett.0c00044
ACS Materials Lett. 2020, 2, 595−601

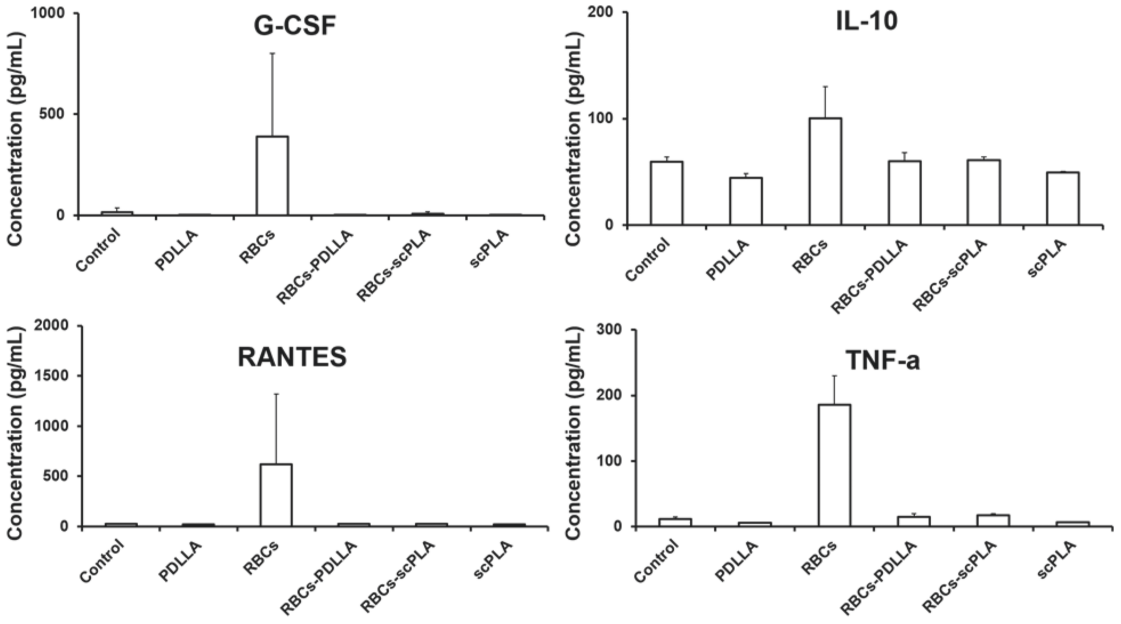

Figure 5. Immunotoxicity assay of RBC-MCNs. The expression of the mouse cytokines, granulocyte-colony-stimulating factor (G-CSF), interleukin (IL)-10, presumably secreted (RANTES), and tumor necrosis factor-α (TNF-α), following the treatment of RAW 264.7 cells with media (control), RBC membrane vesicles, PLAs, and RBC-MCNs tested at a concentration of 5 μg/mL for 24 h.

adapted to encapsulate other cargos, such as different chemotherapeutics, radiosensitizers, and growth factors. Although the cytotoxicity against cancer cells was diminished by packaging the drug within the nanoparticle framework, the extended release profile may be attractive for in vivo efficacy. Therefore, this work represents fundamental advances toward a potential personalized nanocarrier technology that would be capable of employing an individual's RBCs for membrane isolation, together with tuning of cargo loading and release simply via alteration of the biocompatible PLA stereoisomer feed ratio.

■ ASSOCIATED CONTENT

Supporting Information

The Supporting Information is available free of charge at https://pubs.acs.org/doi/10.1021/acsmaterialslett.0c00044.

Experimental procedures, figures, and additional data (PDF)

■ AUTHOR INFORMATION

Corresponding Authors

Lu Su − *Institute for Complex Molecular Systems, Eindhoven University of Technology, 5600, MB, Eindhoven, The Netherlands;* orcid.org/0000-0001-8207-756X; Email: l.su@tue.nl, lusu8487@gmail.com

Karen L. Wooley − *Departments of Chemistry, Chemical Engineering, and Materials Science & Engineering, Laboratory for Synthetic−Biologic Interactions, Texas A&M University, College Station, Texas 77842, United States;* orcid.org/0000-0003-4086-384X; Email: wooley@chem.tamu.edu

Authors

Yen-Nan Lin − *Departments of Chemistry, Chemical Engineering, and Materials Science & Engineering, Laboratory for Synthetic−Biologic Interactions and College of Medicine, Texas A&M University, College Station, Texas 77842, United States*

Mahmoud Elsabahy − *Departments of Chemistry, Chemical Engineering, and Materials Science & Engineering, Laboratory for Synthetic−Biologic Interactions, Texas A&M University, College Station, Texas 77842, United States; Science Academy, Badr University in Cairo (BUC), Badr City 11829, Cairo, Egypt; Department of Pharmaceutics, Faculty of Pharmacy, Assiut University, Assiut 71515, Egypt*

Sarosh Khan − *Departments of Chemistry, Chemical Engineering, and Materials Science & Engineering, Laboratory for Synthetic−Biologic Interactions, Texas A&M University, College Station, Texas 77842, United States*

Fuwu Zhang − *Departments of Chemistry, Chemical Engineering, and Materials Science & Engineering, Laboratory for Synthetic−Biologic Interactions, Texas A&M University, College Station, Texas 77842, United States;* orcid.org/0000-0002-1928-3472

Yue Song − *Departments of Chemistry, Chemical Engineering, and Materials Science & Engineering, Laboratory for Synthetic−Biologic Interactions, Texas A&M University, College Station, Texas 77842, United States;* orcid.org/0000-0002-7800-5528

Mei Dong − *Departments of Chemistry, Chemical Engineering, and Materials Science & Engineering, Laboratory for Synthetic−Biologic Interactions, Texas A&M University, College Station, Texas 77842, United States;* orcid.org/0000-0002-9862-0296

Richen Li − *Departments of Chemistry, Chemical Engineering, and Materials Science & Engineering, Laboratory for Synthetic−Biologic Interactions, Texas A&M University, College Station, Texas 77842, United States*

Justin Smolen − *Departments of Chemistry, Chemical Engineering, and Materials Science & Engineering, Laboratory for Synthetic−Biologic Interactions, Texas A&M University, College Station, Texas 77842, United States*

Rachel A. Letteri − *Department of Chemical Engineering, University of Virginia, Charlottesville, Virginia 22904, United States*

Complete contact information is available at: https://pubs.acs.org/10.1021/acsmaterialslett.0c00044

https://dx.doi.org/10.1021/acsmaterialslett.0c00044
ACS Materials Lett. 2020, 2, 595−601

Notes

The authors declare no competing financial interest.

■ ACKNOWLEDGMENTS

We gratefully acknowledge financial support from the National Science Foundation (CHE-1610311 and DMREF-1629094) and the Robert A. Welch Foundation through the W. T. Doherty-Welch Chair in Chemistry (A-0001). The Laboratory for Synthetic-Biologic Interactions (LSBI) at Texas A&M University is also acknowledged.

■ REFERENCES

(1) Hu, C. M. J.; Zhang, L.; Aryal, S.; Cheung, C.; Fang, R. H.; Zhang, L. F. Erythrocyte Membrane-Camouflaged Polymeric Nanoparticles as a Biomimetic Delivery Platform. *Proc. Natl. Acad. Sci. U. S. A.* **2011**, *108*, 10980−10985.

(2) Kroll, A. V.; Fang, R. H.; Zhang, L. Biointerfacing and Applications of Cell Membrane-Coated Nanoparticles. *Bioconjugate Chem.* **2017**, *28*, 23−32.

(3) Fang, R. H.; Kroll, A. V.; Gao, W.; Zhang, L. Cell Membrane Coating Nanotechnology. *Adv. Mater.* **2018**, *30*, 1706759.

(4) Chen, Y.; Zhang, Y.; Chen, M.; Zhuang, J.; Fang, R. H.; Gao, W.; Zhang, L. Biomimetic Nanosponges Suppress In Vivo Lethality Induced by the Whole Secreted Proteins of Pathogenic Bacteria. *Small* **2019**, *15*, 1804994.

(5) Luk, B. T.; Zhang, L. Cell Membrane-Camouflaged Nanoparticles for Drug Delivery. *J. Controlled Release* **2015**, *220*, 600−607.

(6) Fang, R. H.; Hu, C. M. J.; Luk, B. T.; Gao, W. W.; Copp, J. A.; Tai, Y. Y.; O'Connor, D. E.; Zhang, L. F. Cancer Cell Membrane-Coated Nanoparticles for Anticancer Vaccination and Drug Delivery. *Nano Lett.* **2014**, *14*, 2181−2188.

(7) Hu, C. M. J.; Fang, R. H.; Copp, J.; Luk, B. T.; Zhang, L. F. A Biomimetic Nanosponge that Absorbs Pore-Forming Toxins. *Nat. Nanotechnol.* **2013**, *8*, 336−340.

(8) Thamphiwatana, S.; Angsantikul, P.; Escajadillo, T.; Zhang, Q.; Olson, J.; Luk, B. T.; Zhang, S.; Fang, R. H.; Gao, W.; Nizet, V.; Zhang, L. Macrophage-like nanoparticles concurrently absorbing endotoxins and proinflammatory cytokines for sepsis management. *Proc. Natl. Acad. Sci. U. S. A.* **2017**, *114*, 11488−11493.

(9) Koo, J.; Escajadillo, T.; Zhang, L.; Nizet, V.; Lawrence, S. M. Erythrocyte-Coated Nanoparticles Block Cytotoxic Effects of Group B Streptococcus β-Hemolysin/Cytolysin. *Front. Pediatr.* **2019**, *7*, 410.

(10) Zhang, Q.; Dehaini, D.; Zhang, Y.; Zhou, J.; Chen, X.; Zhang, L.; Fang, R. H.; Gao, W.; Zhang, L. Neutrophil membrane-coated nanoparticles inhibit synovial inflammation and alleviate joint damage in inflammatory arthritis. *Nat. Nanotechnol.* **2018**, *13*, 1182−1190.

(11) Chen, Z.; Zhao, P. F.; Luo, Z. Y.; Zheng, M. B.; Tian, H.; Gong, P.; Gao, G. H.; Pan, H.; Liu, L. L.; Ma, A. Q.; Cui, H. D.; Ma, Y. F.; Cai, L. T. Cancer Cell Membrane-Biomimetic Nanoparticles for Homologous-Targeting Dual-Modal Imaging and Photothermal Therapy. *ACS Nano* **2016**, *10*, 10049−10057.

(12) Kroll, A. V.; Fang, R. H.; Jiang, Y.; Zhou, J.; Wei, X.; Yu, C. L.; Gao, J.; Luk, B. T.; Dehaini, D.; Gao, W.; Zhang, L. Nanoparticulate Delivery of Cancer Cell Membrane Elicits Multiantigenic Antitumor Immunity. *Adv. Mater.* **2017**, *29*, 1703969.

(13) Wei, X.; Zhang, G.; Ran, D.; Krishnan, N.; Fang, R. H.; Gao, W.; Spector, S. A.; Zhang, L. T-Cell-Mimicking Nanoparticles Can Neutralize HIV Infectivity. *Adv. Mater.* **2018**, *30*, 1802233.

(14) Park, J. H.; Dehaini, D.; Zhou, J.; Holay, M.; Fang, R. H.; Zhang, L. Biomimetic nanoparticle technology for cardiovascular disease detection and treatment. *Nanoscale Horiz.* **2020**, *5*, 25−42.

(15) Hu, C.-M. J.; Fang, R. H.; Luk, B. T.; Chen, K. N. H.; Carpenter, C.; Gao, W.; Zhang, K.; Zhang, L. 'Marker-of-self' Functionalization of Nanoscale Particles Through a Top-down Cellular Membrane Coating Approach. *Nanoscale* **2013**, *5*, 2664−2668.

(16) Lee, J. H.; Yeo, Y. Controlled Drug Release From Pharmaceutical Nanocarriers. *Chem. Eng. Sci.* **2015**, *125*, 75−84.

(17) Nyström, A. M.; Xu, Z.; Xu, J.; Taylor, S.; Nittis, T.; Stewart, S. A.; Leonard, J.; Wooley, K. L. SCKs as nanoparticle carriers of doxorubicin: investigation of core composition on the loading, release and cytotoxicity profiles. *Chem. Commun.* **2008**, 3579−3581.

(18) Nyström, A. M.; Wooley, K. L. Construction of thermoresponsive SCKs through tuning the crystalline melting point of the core domain. *Soft Matter* **2008**, *4*, 849−858.

(19) Lin, L. Y.; Lee, N. S.; Zhu, J.; Nyström, A. M.; Pochan, D. J.; Dorshow, R. B.; Wooley, K. L. Tuning core vs. shell dimensions to adjust the performance of nanoscopic containers for the loading and release of doxorubicin. *J. Controlled Release* **2011**, *152*, 37−48.

(20) Drumright, R. E.; Gruber, P. R.; Henton, D. E. Polylactic Acid Technology. *Adv. Mater.* **2000**, *12*, 1841−1846.

(21) Madhavan Nampoothiri, K.; Nair, N. R.; John, R. P. An Overview of the Recent Developments in Polylactide (PLA) Research. *Bioresour. Technol.* **2010**, *101*, 8493−8501.

(22) Tsuji, H. Poly(lactide) Stereocomplexes: Formation, Structure, Properties, Degradation, and Applications. *Macromol. Biosci.* **2005**, *5*, 569−97.

(23) Kang, N.; Perron, M.-È.; Prud'homme, R. E.; Zhang, Y.; Gaucher, G.; Leroux, J.-C. Stereocomplex Block Copolymer Micelles: Core−Shell Nanostructures with Enhanced Stability. *Nano Lett.* **2005**, *5*, 315−319.

(24) Worch, J. C.; Prydderch, H.; Jimaja, S.; Bexis, P.; Becker, M. L.; Dove, A. P. Stereochemical enhancement of polymer properties. *Nat. Rev. Chem.* **2019**, *3*, 514−535.

(25) Shuai, X.; Merdan, T.; Schaper, A. K.; Xi, F.; Kissel, T. Core-Cross-Linked Polymeric Micelles as Paclitaxel Carriers. *Bioconjugate Chem.* **2004**, *15*, 441−448.

(26) Martinez, A. W.; Caves, J. M.; Ravi, S.; Li, W.; Chaikof, E. L. Effects of Crosslinking on the Mechanical Properties, Drug Release and Cytocompatibility of Protein Polymers. *Acta Biomater.* **2014**, *10*, 26−33.

(27) Guo, Z.; Zhao, K.; Liu, R.; Guo, X.; He, B.; Yan, J.; Ren, J. pH-sensitive polymeric micelles assembled by stereocomplexation between PLLA-b-PLys and PDLA-b-mPEG for drug delivery. *J. Mater. Chem. B* **2019**, *7*, 334−345.

(28) Feng, C.; Piao, M.; Li, D. Stereocomplex-Reinforced PEGylated Polylactide Micelle for Optimized Drug Delivery. *Polymers* **2016**, *8*, 165.

(29) Xiao, R. Z.; Zeng, Z. W.; Zhou, G. L.; Wang, J. J.; Li, F. Z.; Wang, A. M. Recent Advances in PEG-PLA Block Copolymer Nanoparticles. *Int. J. Nanomed.* **2010**, *5*, 1057−1065.

(30) Sun, L.; Pitto-Barry, A.; Kirby, N.; Schiller, T. L.; Sanchez, A. M.; Dyson, M. A.; Sloan, J.; Wilson, N. R.; O'Reilly, R. K.; Dove, A. P. Structural reorganization of cylindrical nanoparticles triggered by polylactide stereocomplexation. *Nat. Commun.* **2014**, *5*, 5746.

(31) Hu, C. M. J.; Fang, R. H.; Wang, K. C.; Luk, B. T.; Thamphiwatana, S.; Dehaini, D.; Nguyen, P.; Angsantikul, P.; Wen, C. H.; Kroll, A. V.; Carpenter, C.; Ramesh, M.; Qu, V.; Patel, S. H.; Zhu, J.; Shi, W.; Hofman, F. M.; Chen, T. C.; Gao, W. W.; Zhang, K.; Chien, S.; Zhang, L. F. Nanoparticle Biointerfacing by Platelet Membrane Cloaking. *Nature* **2015**, *526*, 118−121.

(32) Abu Lila, A. S.; Kiwada, H.; Ishida, T. The accelerated blood clearance (ABC) phenomenon: Clinical challenge and approaches to manage. *J. Controlled Release* **2013**, *172*, 38−47.

(33) Zhang, P.; Sun, F.; Liu, S. J.; Jiang, S. Y. Anti-PEG antibodies in the clinic: Current issues and beyond PEGylation. *J. Controlled Release* **2016**, *244*, 184−193.

(34) Tsuji, H.; Hyon, S. H.; Ikada, Y. Stereocomplex Formation Between Enantiomeric Poly(lactic acid)s. 4. Differential Scanning Calorimetric Studies on Precipitates from Mixed Solutions of Poly(D-lactic acid) and Poly(L-lactic acid). *Macromolecules* **1991**, *24*, 5657−5662.

(35) Brizzolara, D.; Cantow, H.-J.; Diederichs, K.; Keller, E.; Domb, A. J. Mechanism of the Stereocomplex Formation between Enantiomeric Poly(lactide)s. *Macromolecules* **1996**, *29*, 191−197.

https://dx.doi.org/10.1021/acsmaterialslett.0c00044
ACS Materials Lett. 2020, 2, 595−601

(36) Sarasua, J. R.; Prud'homme, R. E.; Wisniewski, M.; Le Borgne, A.; Spassky, N. Crystallization and Melting Behavior of Polylactides. *Macromolecules* **1998**, *31*, 3895−3905.
(37) Ikada, Y.; Jamshidi, K.; Tsuji, H.; Hyon, S. H. Stereocomplex formation between enantiomeric poly(lactides). *Macromolecules* **1987**, *20*, 904−906.
(38) Zhang, J.; Sato, H.; Tsuji, H.; Noda, I.; Ozaki, Y. Infrared Spectroscopic Study of CH3···OC Interaction during Poly(l-lactide)/Poly(d-lactide) Stereocomplex Formation. *Macromolecules* **2005**, *38*, 1822−1828.
(39) Leroux, J.-C.; De Jaeghere, F.; Anner, B.; Doelker, E.; Gurny, R. An investigation on the role of plasma and serum opsonins on the evternalization of biodegradable poly(D,L-lactic acid) nanoparticles by human monocytes. *Life Sci.* **1995**, *57*, 695−703.
(40) Saeidlou, S.; Huneault, M. A.; Li, H. B.; Park, C. B. Poly(lactic acid) Crystallization. *Prog. Polym. Sci.* **2012**, *37*, 1657−1677.
(41) Dehaini, D.; Wei, X. L.; Fang, R. H.; Masson, S.; Angsantikul, P.; Luk, B. T.; Zhang, Y.; Ying, M.; Jiang, Y.; Kroll, A. V.; Gao, W. W.; Zhang, L. F. Erythrocyte-Platelet Hybrid Membrane Coating for Enhanced Nanoparticle Functionalization. *Adv. Mater.* **2017**, *29*, 1606209.
(42) Désilets, J.; Lejeune, A.; Mercer, J.; Gicquaud, C. Nano-erythrosomes, a New Derivative of Erythrocyte Ghost: IV. Fate of Reinjected Nanoerythrosomes. *Anticancer Res.* **2001**, *21*, 1741−1747.
(43) Himbert, S.; Alsop, R. J.; Rose, M.; Hertz, L.; Dhaliwal, A.; Moran-Mirabal, J. M.; Verschoor, C. P.; Bowdish, D. M. E.; Kaestner, L.; Wagner, C.; Rheinstädter, M. C. The Molecular Structure of Human Red Blood Cell Membranes from Highly Oriented, Solid Supported Multi-Lamellar Membranes. *Sci. Rep.* **2017**, *7*, 39661.
(44) Elsabahy, M.; Wooley, K. L. Cytokines as Biomarkers of Nanoparticle Immunotoxicity. *Chem. Soc. Rev.* **2013**, *42*, 5552−5576.
(45) Elsabahy, M.; Wooley, K. L. Data Mining as a Guide for the Construction of Cross-Linked Nanoparticles with Low Immunotoxicity via Control of Polymer Chemistry and Supramolecular Assembly. *Acc. Chem. Res.* **2015**, *48*, 1620−1630.
(46) Benne, N.; van Duijn, J.; Kuiper, J.; Jiskoot, W.; Slütter, B. Orchestrating immune responses: How size, shape and rigidity affect the immunogenicity of particulate vaccines. *J. Controlled Release* **2016**, *234*, 124−134.

https://dx.doi.org/10.1021/acsmaterialslett.0c00044
ACS Materials Lett. 2020, 2, 595−601